IET Microwaves, Antennas & Propagation

WILEY

The Institution of Engineering and Technology

ORIGINAL RESEARCH OPEN ACCESS

A High-Efficiency L-Band Planar Array Antenna Using a Shielded Suspended Stripline Feed Network on a Lossy FR-4 Substrate

Soon Young Eom | Dong Pil Chang

Electronics and Telecommunications Research Institute (ETRI), Daejeon, Republic of Korea

Correspondence: Soon Young Eom (syeom@etri.re.kr)

Received: 30 March 2026 | **Revised:** 20 May 2026 | **Accepted:** 9 June 2026

Keywords: microwave antenna arrays | microwave antennas | planar antenna arrays | satellite antennas

ABSTRACT

This paper presents a high-efficiency L-band planar array antenna employing a shielded suspended stripline feed network on a conventional FR-4 substrate. Although achieving high efficiency on FR-4 is generally challenging because of its relatively high dielectric loss tangent, the proposed feed network mitigates substrate loss by realising quasi-air propagation characteristics with an effective permittivity close to unity. The antenna consists of a 6 × 6 planar array of cross-slot-coupled corner-truncated patch elements for left-hand circular polarisation (LHCP), and a sequential rotation feeding scheme based on four quarter subarrays with 90° phase offsets is adopted to improve the axial ratio at the array level. The fabricated antenna uses a 0.2-mm-thick FR-4 PCB integrated with upper and lower metallic shielding enclosures. Experimental results show a measured peak gain of 23.25 dBi and a system-level antenna efficiency exceeding 84% over the operating band from 1.52 to 1.675 GHz, with a boresight axial ratio below 1.51 dB across the entire band. These results confirm that high-efficiency planar array antennas can be realised on a lossy FR-4 substrate, making the proposed design a promising candidate for L-band satellite ground terminal applications.

1 | Introduction

Planar array antennas are widely employed in satellite communication systems owing to their low-profile structure, mechanical robustness, and compatibility with integrated RF front-end circuits [1–4]. In particular, L-band satellite ground terminals and VSAT systems increasingly require planar arrays that provide high radiation efficiency, stable circular polarisation, and sufficient aperture gain while maintaining low fabrication cost and mechanical simplicity. In such systems, antenna efficiency plays a critical role in determining the overall link budget and directly impacts the required output power of high-power amplifiers [5–7].

Conventional planar array antennas commonly employ microstrip-based feeding networks owing to their structural simplicity and ease of integration. However, microstrip feed networks implemented on lossy substrates such as FR-4 suffer from significant dielectric and conductor losses, which severely degrade the overall array efficiency [6–9]. In particular, as the array size increases, the cumulative feeding loss along multi-stage power distribution networks becomes a dominant factor limiting system-level efficiency [1, 2, 6].

To mitigate feeding loss while preserving a planar and low-cost architecture, suspended stripline feeding techniques have been investigated for array antennas [10–14]. By separating the signal conductor from the dielectric substrate, suspended striplines reduce the effective dielectric constant and confine most of the electromagnetic fields within an air region, thereby significantly lowering transmission loss. Alternatively, low-loss feeding structures based on waveguide or substrate-integrated waveguide (SIW) technologies have been proposed [15–18]. However, these approaches generally increase fabrication complexity, structural weight, and cost.

In addition to feeding loss, achieving stable circular polarisation over a wide bandwidth is another critical challenge in planar array antennas. Sequential rotation feeding is a well-established array-level technique that improves polarisation purity and axial ratio bandwidth by properly combining multiple subarrays with progressive phase offsets [19–22]. A preliminary version of this work was presented in [23], where a 4 × 4 planar array antenna using a low-loss HF350F substrate and a shielded suspended stripline feeding network was demonstrated, but relied on a mechanically more elaborate structure, making it less suitable for lightweight and cost-sensitive commercial implementations. In contrast, the present work focuses on a cost-effective implementation using a conventional FR-4 substrate while maintaining high system-level efficiency.

In this context, this paper presents a high-efficiency L-band planar array antenna implemented on a conventional FR-4 substrate using a shielded suspended stripline feeding network. The proposed antenna consists of a 6 × 6 planar array of cross-slot-excited, corner-truncated patch elements to generate left-hand circular polarisation (LHCP). Unlike conventional microstrip-fed arrays, where dielectric loss accumulates rapidly, the proposed architecture confines electromagnetic fields within a quasi-air region, thereby significantly reducing cumulative feeding loss.

Experimental results demonstrate a measured peak gain of 23.25 dBi and an antenna efficiency exceeding 84% over the operating band from 1.52 to 1.675 GHz. These results confirm that high-efficiency planar array antennas can be realised on low-cost lossy substrates through appropriate feeding network design and array-level optimisation.

The main contributions of this work can be summarised as follows:

1. A shielded suspended stripline feeding architecture that suppresses cumulative feeding loss in large-scale planar arrays;
2. Realisation of high-efficiency array operation on a lossy FR-4 substrate through a quasi-air transmission structure;
3. Experimental validation of system-level efficiency exceeding 84% in a full 6 × 6 planar array.

Table 1 [11–15, 23], compares the proposed array antenna with representative suspended-stripline-based planar arrays and related low-loss feeding network approaches, thereby highlighting the contribution of this work.

Notably, a direct comparison of absolute efficiency values is not always straightforward due to differences in array size, operating frequency, and efficiency definition among the reported works. Nevertheless, Table 1 highlights the relative effectiveness of the proposed shielded suspended stripline feeding architecture in realising high-efficiency planar arrays on a lossy FR-4 substrate.

2 | Optimised Design of the Low-Loss Planar Array Antenna

This section describes the optimised design of the proposed high-efficiency 6 × 6 planar array antenna employing a shielded suspended stripline feed network on a lossy FR-4 substrate. First, the design and operating characteristics of the unit radiating element are presented, including the cross-slot coupling structure and circularly polarised patch configuration. Subsequently, the overall array configuration and low-loss feeding architecture are described, with particular emphasis on the sequential rotation feed network and the suppression of cumulative feeding loss in the multi-channel array system.

2.1 | Unit Radiating Element Design

Figure 1 illustrates the exploded three-dimensional structure of the proposed unit radiating element. To implement the shielded suspended stripline–based feeding network, the unit element is configured with upper and lower metallic enclosures. The radiating aperture is formed on the upper enclosure, where an orthogonal cross-slot structure is employed to provide an efficient radiation opening for the suspended patch radiator excited by the shielded suspended stripline feed network. The suspended patch element is located inside a square-shaped internal cavity beneath the cross-slot aperture, and a corner-truncated geometry is adopted to generate left-hand circular polarisation (LHCP).

The cross-slot aperture primarily serves as an electromagnetic coupling and radiation-opening structure rather than as the main circular-polarisation-generating mechanism. Because the suspended patch radiator already supports circular polarisation, the cross-slot dimensions are intentionally designed to provide efficient electromagnetic coupling and stable radiation characteristics while maintaining electromagnetic isolation between the radiating aperture and the shielded suspended stripline feed network. As a result, stable impedance matching and high radiation efficiency are achieved in the proposed unit radiating element.

It should be noted that the primary mechanism responsible for the low-loss performance of the proposed array antenna is the shielded suspended stripline feed network rather than the cavity structure itself. In the proposed configuration, most of the electromagnetic field associated with the feeding network propagates inside the air-filled suspended stripline region, thereby significantly reducing dielectric participation in the lossy FR-4 substrate and enabling quasi-air propagation characteristics.

Meanwhile, the internal cavity surrounding each radiating element mainly serves to provide electromagnetic isolation between adjacent feeding channels and to stabilise the resonant characteristics of the suspended patch radiator. Therefore, the resonance and impedance-matching characteristics of the unit radiating element are determined not only by the physical dimensions of the patch element but also by the dimensions of the internal cavity region and the cross-slot aperture structure.

TABLE 1 | Comparison with prior works.

Ref.	Freq. Band	Array/ Pol.	Feeding network structure	Key results	Main contribution/Limitation
[11]	50–75 GHz	Single/LP	Cavity-backed suspended substrate stripline	Element gain (8–10 dBi)	Foundational SSL antenna/Not array-level
[12]	2.4–2.5 GHz	4 × 4/LP	Suspended stripline-fed printed slot array using low-loss substrate	Gain 18.7 dBi	Early SSL-fed array/Efficiency not emphasized
[13]	9–11 GHz	Subarray/ Dual linear	SSL-fed open-ended metallic waveguide subarray	Isolation focus, $\eta > 69\%$	Phased-array subarray/Not low-cost PCB
[14]	8–12 GHz	Feeding network	Shielded SSL power distribution network using RO4350B substrate	Low loss	Network-level study/No radiation results
[15]	2–3 GHz	4 × 4/LP	Suspended stripline feeding network using low-loss substrate	20–22 dBi (wideband gain)	Different band and implementation
[23]	1.52–1.675 GHz	4 × 4/ LHCP	Shielded suspended stripline feeding network using HF350F substrate with metal enclosure, Sequential rotation	Gain > 20 dBi, $\eta > 92\%$, AR < 1.4 dB	High-efficiency L-band CP array using low-loss HF350F/Mechanically thick and heavy
This work	1.52–1.675 GHz	6 × 6/ LHCP	Shielded suspended stripline feeding network using lossy FR-4 substrate with metal enclosure, Sequential rotation	Gain 23.25 dBi, $\eta > 84\%$, AR < 1.51 dB	High-efficiency L-band CP array using lossy FR-4/Thin and lightweight

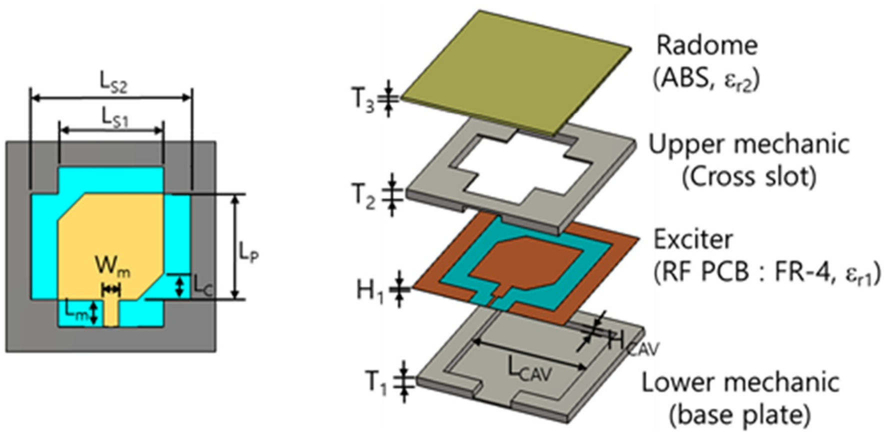

FIGURE 1 | Design parameters and exploded three-dimensional structure of the unit radiating element.

The corner truncation of the square patch element is employed to excite left-hand circular polarisation (LHCP), with approximately 6.3% of the total patch area removed. Although this configuration provides a simple means of realising circular polarisation with a single feed, it generally suffers from a limited axial ratio bandwidth.

To avoid increased structural complexity or degradation in radiation efficiency, the unit radiating element is optimised for high radiation efficiency and stable impedance matching. The circular polarisation performance is instead enhanced at the array level by employing a sequential rotation feeding scheme. Sequential rotation feeding is a well-established technique for improving polarisation purity and axial ratio performance in circularly polarised array antennas [20].

The unit radiating element is optimised to operate over the L-band frequency range from 1.52 to 1.675 GHz, corresponding to a fractional bandwidth of 12.5%, which fully covers the DCS Rx band (1.52–1.525 GHz) and the DCS Tx band (1.67–1.675 GHz). The key design parameters are summarised in Table 2. Since the ground plane size significantly affects the input impedance and radiation characteristics of the unit element, the design is carried out using a sufficiently large ground plane, approximately 1.0 λ_c at the centre frequency, while considering the practical operating environment of the array antenna.

The cross-slot aperture and the internal cavity region directly influence the radiation characteristics of the internally excited patch element and therefore serve as critical design parameters

TABLE 2 | Optimised design parameters and values of the unit radiating element.

Item	Design variables	Design value	Note
Corner-truncated square patch	L_P	79.85 mm	Square patch length
	L_C	21.0 mm	Corner truncation length
	W_m	12.0 mm	Input series stub matching network
	L_m	20.0 mm	
Cross slot	L_{S1}	79.0 mm	Identical horizontal and vertical slot structures
	L_{S2}	120.0 mm	
Mechanics (Aluminium)	T_1	9.0 mm	Thickness of the upper and lower metallic enclosures
	T_2	9.0 mm	
	L_{CAV}	120.0 mm	Square internal cavity length and depth (identical for upper and lower cavities)
	H_{CAV}	7.0 mm	
RF substrate (FR-4)	E_{r1}	4.4	Low-cost thin PCB; T Denotes the copper thickness
	H_1	0.2 mm	
	T	0.018 mm	
Radome	E_{r2}	3.0	ABS material
	T_3	3.0 mm	

together with the patch geometry. Partition walls along the edges of the cross-slot aperture were intentionally omitted to reduce the overall profile height and weight of the array antenna, which are important system-level requirements for satellite ground terminal applications. Although the use of partition walls with a certain height can improve the directivity of a unit element, this approach typically results in increased structural complexity and antenna thickness, and was therefore excluded in the proposed design.

An ABS radome is placed directly on top of the unit radiating element without any air gap. Since the radome thickness is electrically thin compared to the operating wavelength, its impact on the antenna gain is negligible. The radiation loss of the unit element within the operating band is estimated to be less than 0.2 dB, which includes conductor loss (approximately 0.1 dB), dielectric loss from the ABS radome (tanδ ≈ 0.01 at 2 GHz), and dielectric loss from the FR-4 substrate (tanδ ≈ 0.025 at 2 GHz).

The input impedance of the unit radiating element is designed to be 135 Ω. Simulation results with a one-wavelength ground plane show that the input reflection coefficient remains better than −17.1 dB over the entire operating band, indicating good impedance matching as shown in Figure 2.

Figure 3 shows simulated radiation patterns and axial ratio characteristics of the LHCP unit radiating element. The realised gain of the unit radiating element is 8.08 dBi and 8.16 dBi at 1.5225 and 1.6725 GHz, respectively. In contrast, the boresight axial ratio of the unit radiating element is 6.17 dB at 1.5225 GHz and 8.50 dB at 1.6725 GHz, which indicates relatively limited circular polarisation performance.

This behaviour is mainly attributed to the inherently narrow axial ratio bandwidth of the corner-truncated patch structure. Rather than pursuing wideband circular polarisation at the unit-element level, which typically requires additional perturbation

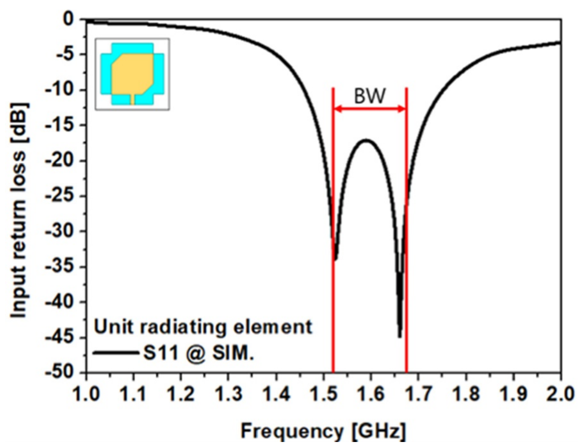

FIGURE 2 | Simulated input return loss of the unit radiating element.

structures or multi-feed configurations that increase conductor loss and fabrication complexity, the unit element is intentionally optimised for high radiation efficiency and stable impedance matching. The limited circular polarisation performance at the unit-element level is therefore compensated at the array level by employing a sequential rotation feeding scheme, as discussed in the following section.

2.2 | Optimised Array Configuration and Low-Loss Feed Network Design

In the proposed planar array antenna, circular polarisation is achieved through a sequential rotation scheme implemented at the array level. Unlike ideal sequential rotation arrays that assume uniform amplitude and phase excitation, the proposed 6 × 6 array operates under non-uniform power division and asymmetric feeding paths imposed by practical size and layout constraints. Therefore, the achieved axial ratio demonstrates the practical effectiveness of the sequential rotation scheme in a realistic array environment using a shielded suspended stripline feed network on a lossy FR-4 substrate. The element spacing of

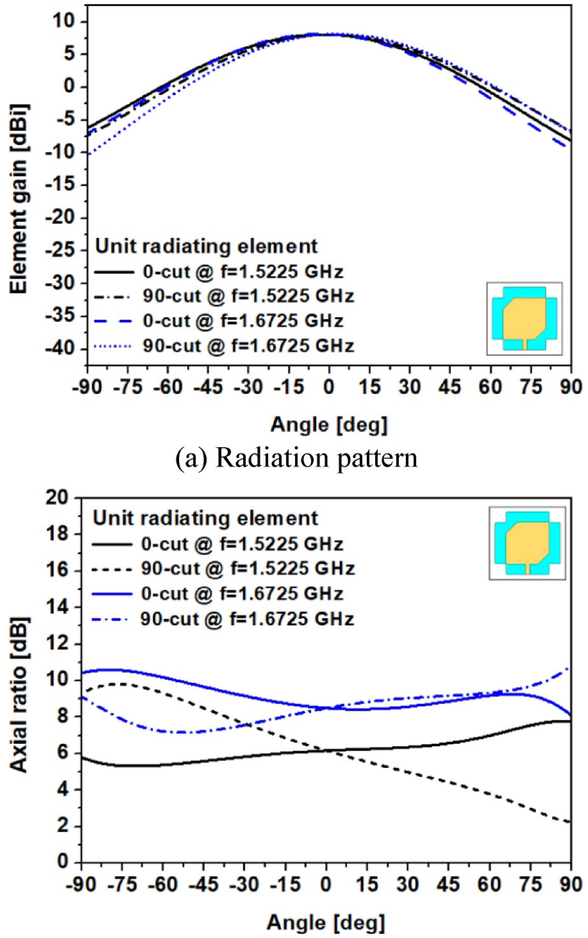

(a) Radiation pattern

(b) Axial ratio

FIGURE 3 | Simulated radiation patterns and axial ratio characteristics of the unit radiating element.

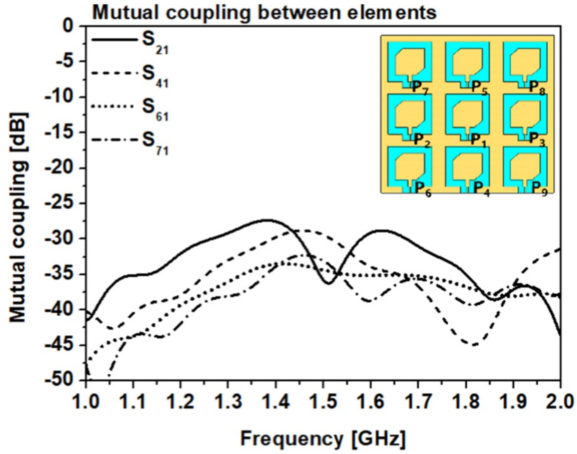

FIGURE 4 | Simulated mutual coupling between elements in a 3 × 3 subarray (element spacing: 157.5 mm).

the proposed 6 × 6 passive array was determined based on the radiation characteristics of the unit radiating element and subsequent electromagnetic verification. An initial spacing was obtained using the unit-element directivity–based guideline given in (1), where the directivity gain of the embedded unit radiating element is 9.11 dBi at 1.5225 GHz and 9.39 dBi at 1.6725 GHz, respectively.

$$d_x \approx \frac{\lambda_c}{2\sqrt{\pi}} 10^{\frac{D_{dBi}}{20}} \quad (1)$$

where λ_c denotes the wavelength at the centre frequency and D_{dBi} represents the directivity of the unit radiating element.

The obtained spacing was validated through electromagnetic verification, including analysis of the effective radiating region, mutual coupling, active input impedance in a 3 × 3 subarray, and ideal multiport pattern synthesis without the feeding network. The selected spacing exhibited sufficiently low inter-element coupling (below approximately −29.0 dB) and followed the expected 10log(N) gain scaling behaviour. Based on these results, the array element spacing was finalised as 157.5 mm, corresponding to approximately 0.84 λ_c at the centre frequency. Figure 4 shows the simulated mutual coupling responses between elements in a 3 × 3 subarray with an element spacing of 157.5 mm, where the centre element is excited. Due to the structural symmetry of the array, the coupling characteristics of S_{31}, S_{51}, S_{81}, and S_{91} are nearly identical to those of S_{21}, S_{41}, S_{61}, and S_{71}, respectively. Therefore, only S_{21}, S_{41}, S_{61}, and S_{71} are presented in Figure 4 for clarity.

The overall physical size of the planar array antenna was constrained to be within 1000 mm × 1000 mm to satisfy practical installation requirements for satellite ground terminal applications. Under this size constraint and the selected element spacing, a 6 × 6 square array configuration was adopted as a practical solution. Although symmetric array configurations generally simplify the feed network design, the chosen 6 × 6 array inevitably results in an asymmetric feeding topology due to geometric and spatial constraints.

In such an asymmetric array configuration, achieving uniform amplitude and phase excitation for all radiating elements requires the use of non-uniform power dividers and additional phase-matching networks. These components compensate for unequal electrical path lengths and spatial constraints imposed by the compact array layout. Figure 5 illustrates the conceptual power distribution architecture proposed for the 6 × 6 square planar array antenna.

To achieve excellent axial ratio performance in the overall array antenna, the proposed 6 × 6 planar array is divided into four quarter subarrays (QA-1 to QA-4), each of which is sequentially rotated by 90° with respect to a reference orientation. A relative 90° phase difference between the rotated subarrays is introduced by a four-way power divider located at the input stage. Through this sequential rotation scheme, the limited circular polarisation performance of the individual radiating elements is effectively compensated at the array level. To uniformly distribute power to the 3 × 3 elements within each quarter subarray, non-uniform T-junction power dividers are employed, including a three-way divider with a 4:3:2 power ratio and a two-way divider with a 2:1 power ratio. These non-uniform power division ratios arise from the asymmetric geometry and spatial constraints of the compact 6 × 6 array configuration. To ensure coherent phase excitation across all radiating elements, additional delay lines corresponding to one guided wavelength

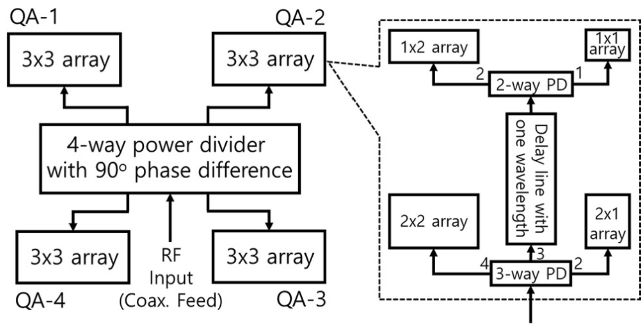

FIGURE 5 | Power distribution configuration for the 6 × 6 array antenna.

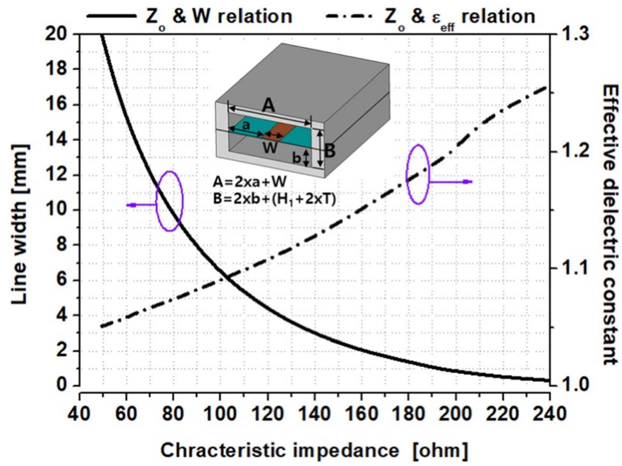

FIGURE 6 | Relationship between line width and effective permittivity as a function of characteristic impedance.

at the centre frequency are introduced along each feeding path, resulting in equal phase conditions at all element ports.

To realise a planar array antenna with high radiation efficiency and stable radiation characteristics, a shielded suspended stripline–based feeding network is adopted in this study. Using a thin FR-4 substrate with a thickness of 0.2 mm, the relationship between the characteristic impedance, line width, and equivalent effective permittivity of the shielded suspended stripline is investigated, as shown in Figure 6. The results in Figure 6 are extracted under structural parameters of a = 12.0 mm and b = 7.0 mm. Owing to the sufficiently large cross-sectional dimensions of the suspended stripline structure, the equivalent effective permittivity is maintained in a low range of 1.05–1.26, which effectively mitigates the dielectric loss typically associated with FR-4 substrates and enables low-loss power distribution in the proposed array antenna.

Figure 7 illustrates the configuration of the optimally designed 6 × 6 square planar array antenna. Full-wave electromagnetic simulations confirm that the mutual coupling between adjacent array elements is suppressed below −28.7 dB across the entire operating band, which is sufficiently low for stable array operation. This low mutual coupling level is mainly attributed to the cavity-backed element structure and the electromagnetic isolation provided by the shielded suspended stripline feeding network.

The overall planar array antenna is composed of three distinct layers: an upper metallic enclosure that serves as the common ground plane for the cross-slot radiating aperture and the feeding network, a middle layer containing the shielded suspended stripline–based feed network, and a lower metallic enclosure acting as the bottom ground plane of the feed network. In this configuration, the upper and lower metallic enclosures provide electromagnetic shielding for the feeding network in the vertical direction, effectively suppressing undesired radiation and parasitic coupling. Meanwhile, the shielded suspended stripline in the middle layer transfers electromagnetic energy to the radiating elements while remaining electromagnetically isolated from the radiating aperture, thereby enabling high-efficiency and low-loss array antenna operation. The RF PCB used to implement the shielded suspended stripline feed network is fabricated on an FR-4 substrate with a relative permittivity of 4.4, a thickness of 0.2 mm, a copper thickness of 0.018 mm, and a loss tangent of 0.025 at 2 GHz.

To achieve wideband circular polarisation performance, four quarter subarrays (QA-1 to QA-4) are sequentially rotated by 90° with respect to a reference orientation, as shown in Figure 7c. This sequential rotation configuration effectively compensates for the limited circular polarisation characteristics of the individual radiating elements at the array level, resulting in a significant improvement in the overall axial ratio. The input four-way power divider is located at the centre of the array antenna and is excited through a coaxial feed using a 50-Ω SMA (female) connector. The input impedance at each of the four output ports is designed to be 200 Ω, which is achieved by employing quarter-wavelength impedance transformers with a characteristic impedance of 192.4 Ω. To accommodate spatial constraints in the feeding network, a meander-line transmission-line structure is adopted to implement the required 90° phase differences between the quarter subarrays.

Figure 8 illustrates the complete layout configuration of the proposed 1-to-36 shielded suspended stripline feed network. Port P_1 denotes the input excitation port, whereas ports P_2–P_{37} correspond to the 36 output ports connected to the radiating elements. The proposed feed network consists of an input 1-to-4 sequential rotation divider and four non-uniform 1-to-9 subarray feed networks. All 36 output channels are designed to provide equal-amplitude excitation. The four quarter subarrays (QA-1 to QA-4) have identical feed-network configurations rotated sequentially by 90° with respect to each other. Accordingly, the input 1-to-4 power divider provides sequential phase excitations with 90° phase progression in the clockwise direction.

To realise the required sequential phase excitation within the limited layout area of the compact 6 × 6 planar array, compact meander-line delay sections are introduced in the feeding network. In the complete 1-to-36 feed network, the shortest transmission paths, corresponding to the P_1–P_2, P_1–P_4, P_1–P_8, and P_1–P_9 channels, have an electrical length of approximately 4.14 λ_g, whereas the longest transmission path, corresponding to the P_1–P_{34} channel, has an electrical length of approximately 6.39 λ_g at the centre frequency.

Although meander-line phase shifters provide a compact and simple implementation, their phase-delay characteristics are

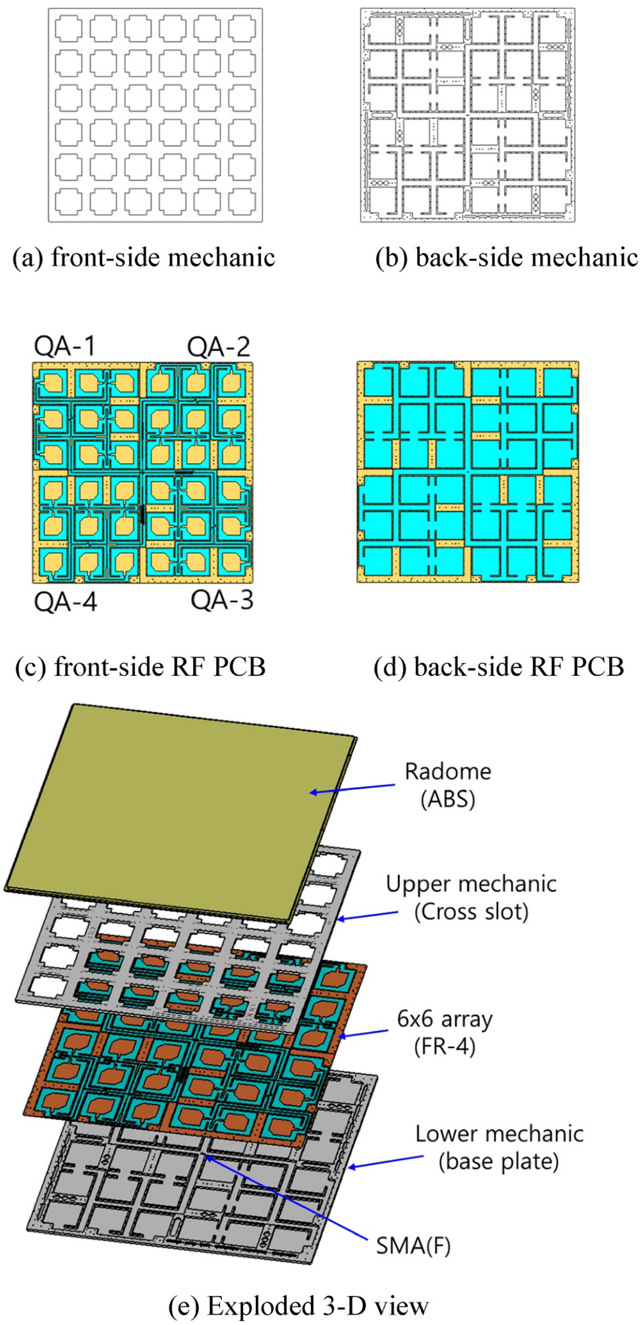

FIGURE 7 | Configuration of the optimally designed 6 × 6 square array antenna.

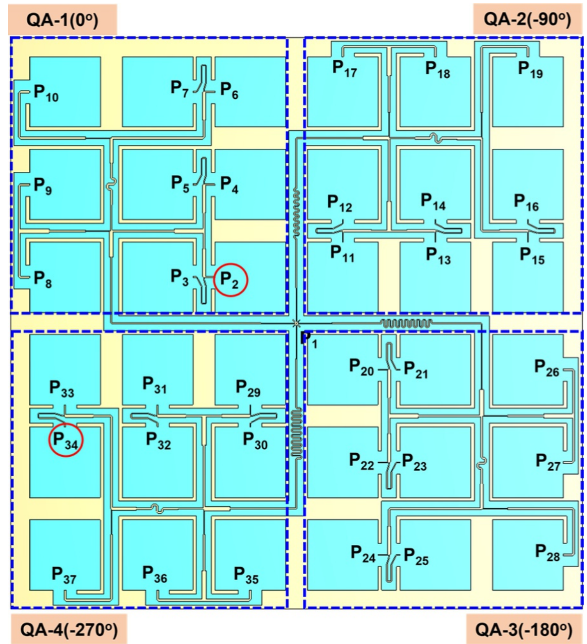

FIGURE 8 | Layout configuration of the complete 1-to-36 shielded suspended stripline feed network.

inherently frequency-dependent because of the folded transmission-line geometry. In particular, the phase delay designed at the centre frequency may vary nonlinearly towards the band edges, potentially leading to increased phase imbalance in array antennas. In circularly polarised array antennas, phase errors between adjacent radiating elements or subarrays can degrade the orthogonality between the two orthogonal field components, which is a primary cause of axial-ratio deterioration. While ideal circular polarisation requires equal amplitudes and an exact 90° phase difference between the orthogonal field components, phase imbalance introduced by the feeding network can disrupt this condition and increase elliptically polarised components. This effect becomes more pronounced as the number of array elements increases because of cumulative phase dispersion. Therefore, the phase matching accuracy of the feeding network plays a critical role in determining the axial-ratio performance of the overall array antenna.

Simulation results confirm that the proposed feeding network provides sufficiently stable amplitude and phase characteristics over the operating band despite the use of compact meander-line phase-delay sections. As a result, the relatively degraded axial ratio observed at the unit-element level is effectively compensated at the array level, yielding excellent axial-ratio performance over the operating band.

To further investigate the electrical performance of the proposed feed network, full-wave electromagnetic simulations were carried out for the individual 1-to-4 divider, the 1-to-9 subarray feed network, and the complete 1-to-36 feed network. Figure 9 shows the simulated insertion loss and phase characteristics of the proposed feed networks, while the corresponding quantitative performance metrics are summarised in Table 3.

For the input 1-to-4 power divider, the average insertion loss is 6.15 dB over the operating band, corresponding to an excess feeding loss of approximately 0.13 dB compared with the ideal 6.02 dB power-division loss. The simulated amplitude deviation remains within ± 0.36 dB with an RMS variation of 0.22 dB. Owing to the use of compact meander-line phase-delay sections, the phase deviation gradually increases towards the band edges, reaching a maximum deviation of approximately +28.49° at the upper operating frequency.

For the 1-to-9 feed network used in each quarter subarray, the average insertion loss is 9.77 dB, corresponding to an excess feeding loss of approximately 0.23 dB relative to the ideal 9.54 dB division loss. The RMS amplitude and phase deviations are 0.42 dB and 9.56°, respectively. These results indicate that the proposed non-uniform feed network maintains

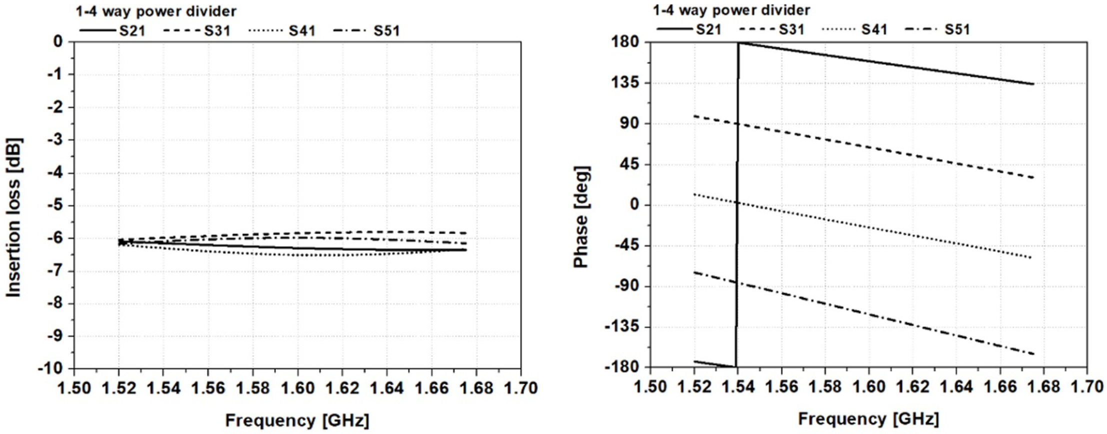

(a) 1-to-4 divider

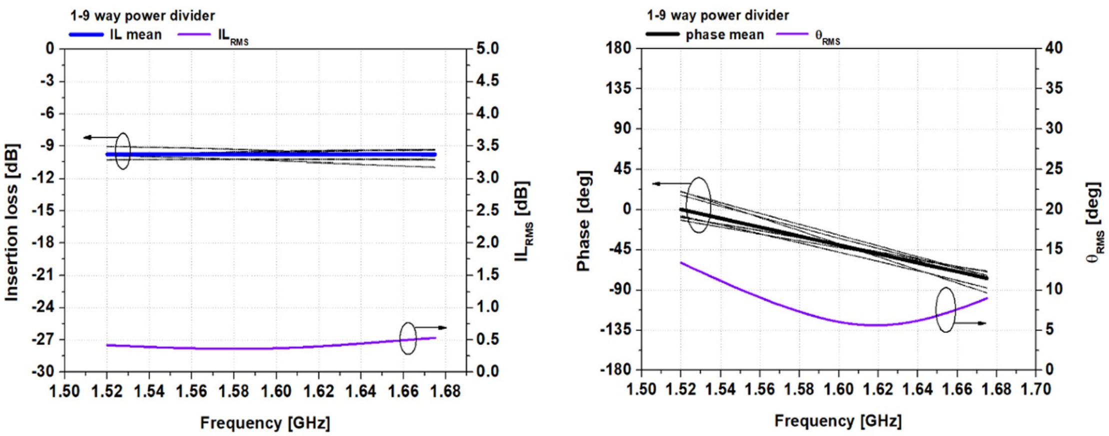

(b) 1-to-9 divider

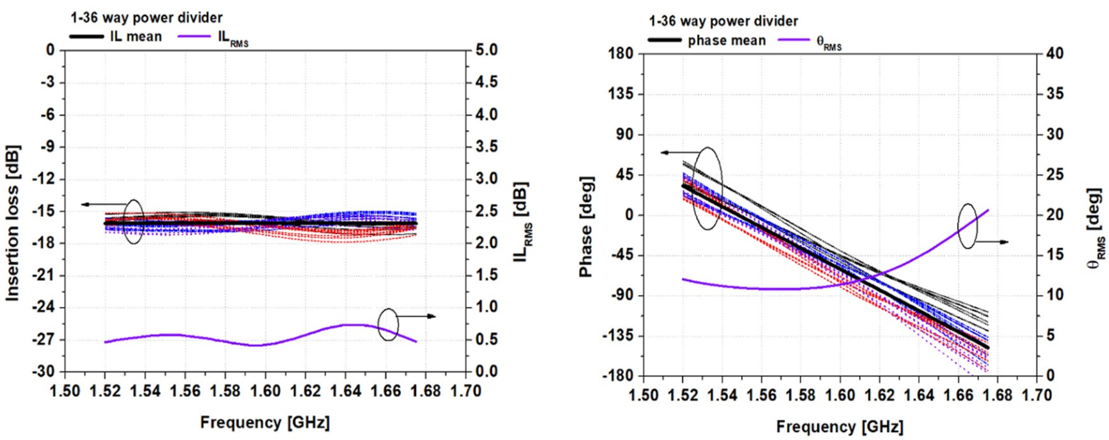

(c) complete 1-to-36 feed network

FIGURE 9 | Simulated insertion-loss and phase characteristics of the proposed feed networks.

sufficiently stable amplitude and phase characteristics for practical sequentially rotated array operation.

Finally, the complete 1-to-36 feed network exhibits an average insertion loss of 16.11 dB, corresponding to an excess feeding loss of only 0.55 dB beyond the ideal 15.56 dB power-division loss. The RMS amplitude deviation is 0.57 dB, while the RMS phase deviation is 13.1° over the operating band. Because the proposed array employs simple meander-line delay sections to realise the required 90° sequential phase excitation under limited layout space, the phase delay becomes increasingly frequency-dependent towards the band edges over the 9.7%

TABLE 3 | Simulated insertion-loss and phase-balance performance of the proposed shielded suspended stripline feed networks.

Feed network	Ideal division loss (dB)	Mean insertion loss (dB)	Excess feeding loss (dB)	RMS amplitude deviation (dB)	RMS phase deviation
1-to-4 divider	6.02	6.15	0.13	0.22	Path-dependent, up to +28.49°
1-to-9 subarray network	9.54	9.77	0.23	0.42	9.56°
Complete 1-to-36 network	15.56	16.11	0.55	0.57	13.1°

operating bandwidth. This frequency-dependent phase dispersion is considered one of the main factors responsible for the residual axial-ratio degradation observed in the measured array, although the measured boresight axial ratio remains below 1.51 dB across the entire operating band.

These results confirm that the proposed shielded suspended stripline feed network achieves low-loss multi-channel power distribution while maintaining sufficiently stable amplitude and phase characteristics for high-efficiency circularly polarised array operation.

The overall simulation results of the 6 × 6 square planar array antenna are presented and compared with the measured results in Section 3.

3 | Fabrication and Experimental Results

Figure 10 shows a photograph of the fabricated L-band 6 × 6 square planar array antenna. The external radome is fabricated from ABS material with a thickness of 3.0 mm. The overall dimensions of the antenna, including the radome, are 994 × 994 × 22 mm^3, which correspond to 5.29 λ_c × 5.29 λ_c × 0.12 λ_c at the centre frequency. Owing to its low-profile height of only 0.12 λ_c, the proposed planar array antenna offers a significant reduction in thickness compared to conventional reflector antennas. This low-profile configuration provides practical advantages for satellite ground terminal applications, including reduced installation space requirements and improved mechanical stability under outdoor operating conditions.

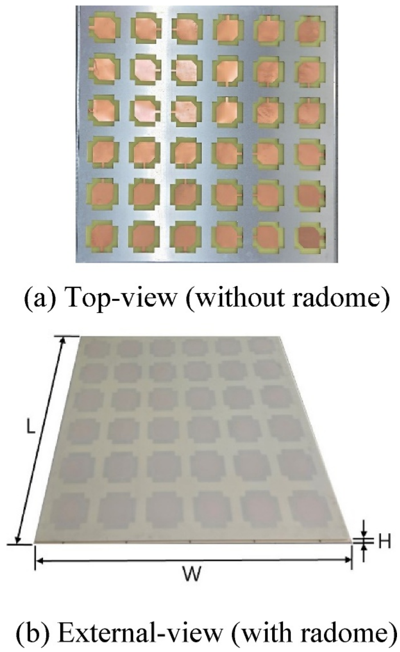

FIGURE 10 | Photograph of the fabricated 6 × 6 square array antenna.

The measured input return loss of the L-band planar array antenna is presented in Figure 11. The measured results show close agreement with the full-wave electromagnetic simulation, validating the accuracy of the proposed design. Across the entire operating frequency band, the measured return loss remains better than −19.1 dB, indicating excellent input impedance matching, which is essential for minimising reflection loss and achieving high radiation efficiency.

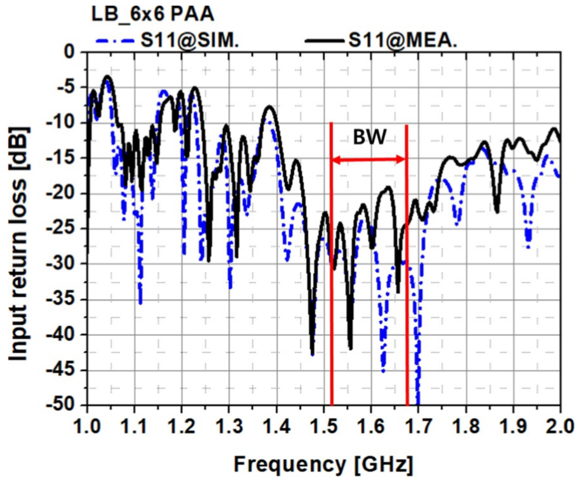

FIGURE 11 | Measured and simulated input return loss of the L-band planar array antenna.

Figure 12 presents the measured radiation characteristics of the L-band 6 × 6 square planar array antenna obtained in a fully anechoic chamber. The measured radiation patterns exhibit symmetric and well-defined main beams, showing close agreement with the corresponding full-wave electromagnetic simulation results. Moreover, clearly defined nulls consistent with the expected array factor distribution are observed in the measured patterns, which confirms the accuracy of the amplitude and phase distributions provided by the designed feeding network. Figure 13 shows the gain characteristics of the 6 × 6 square array antenna as a function of frequency. It can be observed that the measured gain at 1.5225, 1.5975, and 1.6725 GHz agrees well with the simulated gain. Figure 14 shows the measured axial ratio characteristics of the 6 × 6 square planar array antenna at 1.5225 and 1.6725 GHz.

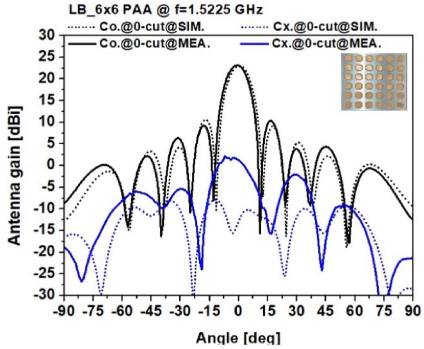

(a) 0°-cut @ f=1.5225 GHz

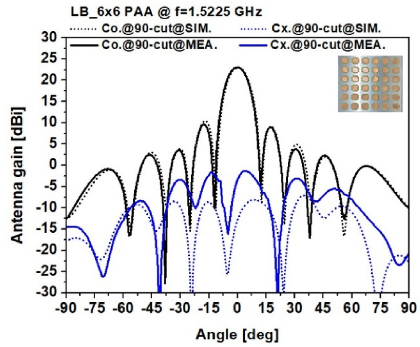

(b) 90°-cut @ f=1.5225 GHz

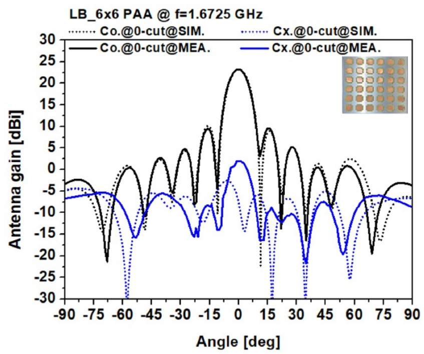

(c) 0°-cut @ f=1.6725 GHz

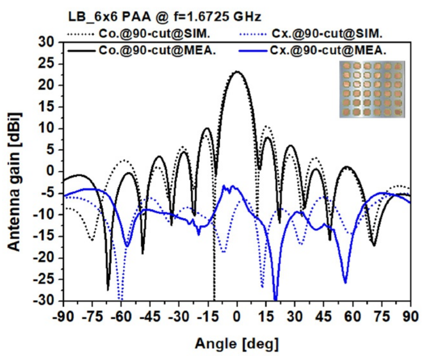

(d) 90°-cut @ f=1.6725 GHz

FIGURE 12 | Measured radiation characteristics of the 6 × 6 square array antenna.

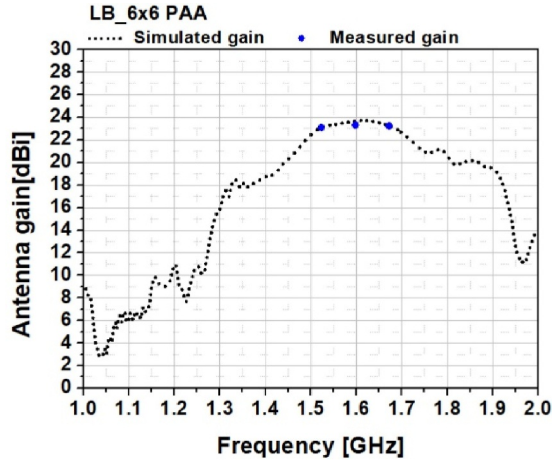

FIGURE 13 | Gain characteristics of the 6 × 6 square array antenna as a function of frequency.

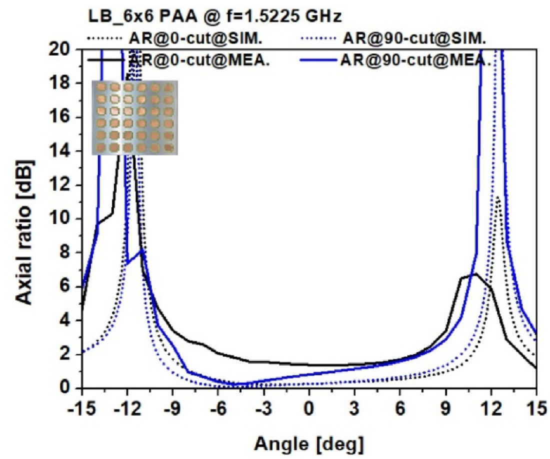

(a) Axial ratio @ f=1.5225 GHz

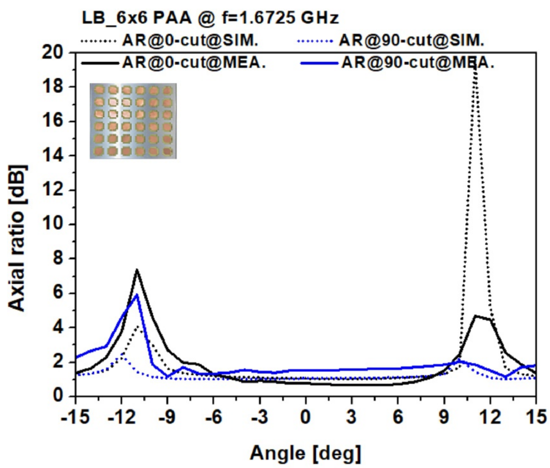

(b) Axial ratio @ f=1.6725 GHz

FIGURE 14 | Axial ratio characteristics of the 6 × 6 square array antenna.

The key measured radiation characteristics of the L-band 6 × 6 square planar array antenna are summarised in Table 4. The measured boresight axial ratio is 1.40 dB at 1.5225 GHz and 1.51 dB at 1.6725 GHz, remaining below 1.51 dB over the entire operating band. These results verify the effectiveness of the proposed sequential rotation feeding scheme in compensating for the limited circular-polarisation performance of the individual radiating elements and achieving stable array-level circular polarisation characteristics.

TABLE 4 | Summary of radiation characteristics of the 6 × 6 square array antenna.

Item	Simulation	Measurement
Operating band	1.52–1.675 GHz	1.52–1.675 GHz
Antenna gain	23.1 dBi @1.5225 GHz(Rx) 23.3 dBi @1.6725 GHz(Tx)	23.12 dBi @1.5225 GHz(Rx) 23.25 dBi @1.6725 GHz(Tx)
3-dB Beamwidth	10.6° typ. @1.5225 GHz(Rx) 9.8° typ. @1.6725 GHz(Tx)	10.6° typ. @1.5225 GHz(Rx) 9.8° typ. @1.6725 GHz(Tx)
Sidelobe level	12.4 dB Min. @1.5225 GHz 12.6 dB Min. @1.6725 GHz	12.8 dB Min. @1.5225 GHz 13.1 dB Min. @1.6725 GHz
Polarisation	LHCP	LHCP
Axial ratio (boresight)	0.28 dB @1.5225 GHz 0.49 dB @1.6725 GHz	1.40 dB @1.5225 GHz 1.51 dB @1.6725 GHz
Antenna efficiency	85.7% @1.5225 GHz (−0.67 dB) 85.1% @1.6725 GHz (−0.70 dB)	86.1% @1.5225 GHz (−0.65 dB) 84.1% @1.6725 GHz (−0.75 dB)

These results indicate that the shielded suspended stripline feed network introduces only 0.55 dB of excess feeding loss in the complete 1-to-36 distribution network, despite the use of a lossy FR-4 substrate. Therefore, the measured system-level antenna efficiency exceeding 84% is physically consistent with the low simulated feed-network loss.

The total system-level loss, including the loss of the shielded suspended stripline feeding network, conductor and dielectric losses of the unit radiating elements, and impedance mismatch loss, is estimated to be less than 0.75 dB. In addition, the reported array efficiency inherently includes degradation associated with amplitude and phase imbalance in the 6 × 6 multichannel array excitation.

As a result, the proposed 6 × 6 planar array antenna achieves a high antenna efficiency exceeding 84%, despite the use of a lossy FR-4 substrate. The array antenna efficiency is evaluated from the ratio between the measured realised gain and the simulated directivity of the complete array antenna, where the difference between these two quantities represents the overall system-level loss [24]. Therefore, the reported efficiency inherently accounts for conductor loss, dielectric loss, feeding-network loss, impedance mismatch loss, and degradation associated with non-ideal array excitation conditions.

4 | Conclusion

A high-efficiency L-band planar array antenna employing a shielded suspended stripline feed network on a conventional lossy FR-4 substrate has been presented. The adopted 6 × 6 array configuration represents a practical trade-off among aperture gain, feeding network complexity, and mechanical size for L-band satellite ground terminal applications.

Despite the inherently high dielectric loss of FR-4, the proposed feeding architecture effectively mitigates substrate loss by confining electromagnetic fields within a shielded air-filled cavity. The fabricated 6 × 6 array achieves a measured peak gain of 23.25 dBi and an efficiency exceeding 84% over the operating band from 1.52 to 1.675 GHz, demonstrating experimentally validated system-level efficiency, including feeding, matching, and array combining effects.

The measured axial ratio remained below 1.51 dB across the entire band and showed good agreement with full-wave simulations. These results confirm that high-efficiency planar array antennas can be realised on a lossy FR-4 substrate, making the proposed design a promising candidate for L-band satellite ground terminal and VSAT applications.

Author Contributions

Soon Young Eom: conceptualization, investigation, methodology, validation, writing – original draft, writing – review and editing. **Dong Pil Chang:** funding acquisition, project administration, writing – review and editing.

Acknowledgements

This work was supported by Institute for Information & communications Technology Planning & Evaluation (IITP) grant funded by the Korean Government (MSIT) (No. 2018-0-00190, Development of Core Technology for Satellite Payload).

Conflicts of Interest

The authors declare no conflicts of interest.

Data Availability Statement

The data that support the findings of this study are available from the corresponding author upon reasonable request.

References

1. D. M. Pozar, "Microstrip Array Antennas," *Proceedings of the IEEE* 80, no. 1 (1992): 79–91, https://doi.org/10.1109/5.119568.

2. R. J. Mailloux, *Phased Array Antenna Handbook* (Artech House, 2005).

3. C. A. Balanis, *Antenna Theory: Analysis and Design*. 3rd ed. (Wiley, 2005).

4. R. C. Hansen, *Phased Array Antennas*. 2nd ed. (Wiley, 2009).

5. T. S. Rappaport, *Wireless Communications: Principles and Practice*. 2nd ed. (Prentice Hall, 2002).

6. D. R. Jackson and N. G. Alexopoulos, "Simple Approximate Formulas for Input Resistance, Bandwidth, and Efficiency of a Resonant

Rectangular Patch," *IEEE Transactions on Antennas and Propagation* 39, no. 3 (1991): 407–410, https://doi.org/10.1109/8.76341.

7. K. L. Wong, *Compact and Broadband Microstrip Antennas* (Wiley, 2002).

8. J. Huang, "The Finite Ground Plane Effect on Microstrip Antenna Radiation Patterns," *IEEE Transactions on Antennas and Propagation* 31, no. 4 (1983): 649–653, https://doi.org/10.1109/tap.1983.1143108.

9. E. O. Hammerstad and O. Jensen, *Accurate Models for Microstrip computer-aided Design* (IEEE MTT-S Int. Microwave Symp. Dig., 1980), 407–409.

10. S. D. Targonski, R. B. Waterhouse, and D. M. Pozar, "Wideband Aperture-Coupled Stacked Patch Antenna Using Thick Substrates," *Electronics Letters* 32, no. 21 (1996): 1941–1942, https://doi.org/10.1049/el:19961306.

11. R. N. Simons, *A millimeter-wave cavity-backed Suspended Substrate Stripline Antenna* (NASA Technical Memorandum, 1999).

12. J. He, X. Chen, and K. Huan, "A Novel Suspended Stripline-Fed Printed Square Slot Array Antenna With High Gain," *International Journal of RF and Microwave Computer-Aided Engineering* 19, no. 6 (2009): 712–716, https://doi.org/10.1002/mmce.20395.

13. N. Nakamoto, T. Takahashi, T. Fukasawa, N. Yoneda, and H. Miyashita, "A Suspended Stripline-Fed Dual-Polarized Open-Ended Waveguide Subarray With Metal Posts for Phased Array Antennas," *IEICE Transactions on Communications* E104-B, no. 3 (2021): 295–303, https://doi.org/10.1587/transcom.2020ebp3067.

14. J. M. Inclán-Alonso, J. M. Fernández-González, and M. Sierra-Pérez, "Low-Loss Power Distribution Network in Stripline Technology for Planar Array Antennas," *Progress in Electromagnetics Research* 143 (2013): 369–384, https://doi.org/10.2528/pier13061107.

15. N. Daviduvitz, U. Zohar, and R. Shavit, "Wideband and High-Gain Planar Array With a Suspended Stripline Feeding Network," in *Proc. IEEE Int. Conf. Microwaves, Communications, Antennas and Electronic Systems (COMCAS)* (2011), 1–5.

16. Y. Cassivi, L. Perregrini, P. Arcioni, M. Bressan, and K. Wu, "Dispersion Characteristics of Substrate Integrated Rectangular Waveguide," *IEEE Microwave and Wireless Components Letters* 12, no. 9 (2002): 354–356, https://doi.org/10.1109/LMWC.2002.803188.

17. D. Deslandes and K. Wu, "Integrated Microstrip and Rectangular Waveguide in Planar Form," *IEEE Microwave and Wireless Components Letters* 11, no. 2 (2001): 68–70, https://doi.org/10.1109/7260.914305.

18. M. Bozzi, A. Georgiadis, and K. Wu, "Review of Substrate-Integrated Waveguide Circuits and Antennas," *IET Microwaves, Antennas and Propagation* 5, no. 8 (2011): 909–920, https://doi.org/10.1049/iet-map.2010.0463.

19. J. Hirokawa and M. Ando, "Single-Layer Feed Waveguide Consisting of Posts for Plane TEM Wave Excitation in Parallel Plates," *IEEE Transactions on Antennas and Propagation* 46, no. 5 (1998): 625–630, https://doi.org/10.1109/8.668903.

20. J. Huang, "A Technique for an Array to Generate Circular Polarization With Linearly Polarized Elements," *IEEE Transactions on Antennas and Propagation* 34, no. 9 (1986): 1113–1124, https://doi.org/10.1109/tap.1986.1143953.

21. A. Chen, C. Yang, Z. Chen, Y. Zhang, and Y. He, "Design of Multilevel Sequential Rotation Feeding Networks Used for Circularly Polarized Microstrip Antenna Arrays," *International Journal of Antennas and Propagation* 2012 (2012): 10, https://doi.org/10.1155/2012/304816.

22. S. Gao, Q. Luo, and F. Zhu, *Circularly Polarized Antennas* (Wiley, 2014).

23. S. Y. Eom and D. P. Chang, "L-Band Planar Array Antenna With High Efficiency for DCS_VSAT Applications," in *Proc. Int. Conf. Information and Communication Technology Convergence (ICTC)* (Jeju, 2023), 1640–1641.

24. D. M. Pozar, *Microwave Engineering*. 4th ed. (Wiley, 2011).